Indian Journal of Pure & Applied Physics
Vol. 54, October 2016, pp. 665-675

Nonlinear stability and failure analysis of perforated FGM plate

Kanishk Sharma* & Dinesh Kumar

Mechanical Engineering Department, Malaviya National Institute of Technology, Jaipur 302 017, India

Received 5 January 2016; revised 2 August 2016; accepted 11 August 2016

A nonlinear finite element analysis, based on the first-order shear deformation theory and the von-Karman's nonlinear kinematics, of Ti/TiB FGM plate with a central circular hole under in-plane compressive load has been presented. The volume fractions of FGM constituents (ceramic and metal) have been varied according to simple power law distribution in the thickness direction of FGM plate. The actual non-homogeneous FGM plate with continuously varying properties along thickness has been modeled as a laminate composed of multiple perfectly-bonded layers of isotropic material having layer-wise homogenous composition. The FGM material has been assumed to be graded as per TTO model (i.e., the modified rule of mixtures) to calculate the Young's modulus and the yield strength of FGM plate at a particular thickness coordinate. The failure of the FGM plate has been predicted by applying 3-D von-Mises criterion. After validating the results of present formulation with that reported in the literature, various numerical studies have been conducted to examine the effects of different parameters, viz, material in-homogeneity, slenderness ratio, boundary conditions, hole-size and loading conditions on the bucking and postbuckling behavior, and the failure response of FGM plate. It has been concluded that clamped FGM plate with large hole-size possesses more buckling load than with a small hole-size because of the rigid boundary edge conditions, whereas failure load and associated maximum transverse deflection as well as the postbuckling stiffness of FGM plate monotonically decrease with the increase in hole-size. It has been envisioned that the present study would provide an enhanced insight into the stability and failure behavior of perforated FGM structures.

Keywords: Nonlinear analysis, Postbuckling, Functionally graded material (FGM), Finite element method (FEM), FGM failure, FGM plate with hole

1 Introduction

In recent years, lots of research has been focused on the development of new and efficient materials and on the use of these new materials to optimize the design of structures for various engineering applications with enhanced performance. At present, thin laminated composite plates/shells are widely used in various diverse engineering applications, such as high-speed flights and aircrafts, spacecrafts, nuclear reactors, satellites, defense vehicles, as the main load carrying members because of their high specific strength and stiffness. But, now-a-days functionally graded materials (FGMs), an advanced inhomogeneous composite materials with continuously and smoothly varying material properties, along a particular and predefined direction(s), obtained by gradually altering the volume fraction of the constituents materials (usually ceramic and metal), are finding increasing applications in numerous engineering fields because of the absence of interface problems (cracking and debonding/delamination) prevailing in conventional composite structures at high thermo-mechanical loading conditions[1,2]. Moreover, FGMs also possess, besides the flexibility to tailor the internal composition to meet the design requirements, other unique and outstanding properties such as high fracture toughness, thermal resistance along with desired structural integrity and high heat-shielding properties, which make them suitable for different applications[3,4].

Thin walled members, such as plates and shells used extensively in various engineering applications, are more susceptible to buckling, large amplitude deflections, or excessive stresses under different in-plane mechanical and/or thermal loading conditions. It is well known that under in-plane loading (compression and/or shear) conditions, plate like structures are designed efficiently by utilizing the postbuckling reserve strength possessed beyond buckling[5,6]. Moreover, holes or cutouts are often made into plates for various practical needs such as ports to provide access to mechanical and electrical systems, holes for damage inspections, and cutouts/holes to serve as doors and windows, etc[7–10]. However, the presence of these cutouts/holes changes the buckling

*Corresponding author (E-mail: kanishksharma2009@gmail.com)

characteristics and load carrying capacity of the plate drastically. Therefore, to make use of a new material like FGM in an efficient and economical manner, it is very essential to analyze and gain a thorough knowledge of responses, such as buckling and postbuckling behavior and failure, of various basic structural elements, such as thin plates with a hole, made of FGM under various in-plane loads.

Numerous studies pertaining to structural analysis of FGM plate, involving thermal stress, vibration, buckling, static and dynamic analysis, have been carried out to date. Stability analysis of FGM plates is of great concern and in recent years, many studies have been performed in this area. Birman[11] made the first attempt to solve the buckling problem of functionally graded hybrid composite plates. Feldman and Aboudi[12] studied the elastic bifurcational buckling of functionally graded SiC/Al plate under in-plane compressive loading. In addition, there are numerous works devoted only to buckling analysis of FGM plates under various mechanical and/or thermal loads[13–17].

Many researchers have also conducted various postbuckling analysis of FGM plates under thermal and/or mechanical loads. Liew *et al*[18] examined the postbuckling behavior of functionally graded rectangular plates integrated with surface-bonded piezoelectric actuators using the Reddy's higher-order shear deformation plate theory. Yang and Shen[19] developed a semi-numerical approach using perturbation technique in conjunction with one-dimensional differential quadrature approximation and Galerkin procedure to study the large deflection and postbuckling responses of FGM rectangular plates under transverse and in-plane mechanical loads. An analytical solution to study the postbuckling behavior of moderately thick FGM plates and shallow shells under edge compressive loads and a temperature field was developed by Woo *et al*[20]. Using 3-D finite element method, Na and Kim[21,22] conducted 3D thermal buckling and postbuckling analysis of FGM plates with temperature dependent material properties, subjected to uniform and non-uniform temperature rise. Shen[23] presented the thermal postbuckling analysis of a simply-supported, shear deformable FGM plates with temperature-dependent properties. The stability of simply-supported rectangular FGM plates with temperature dependent material properties, under in-plane thermomechanical loading was investigated by Duc and Tung[24]. The material properties are assumed to be temperature-dependent and graded in the thickness direction according to a simple power-law distribution in terms of volume fractions of constituents. Wu *et al*[25] predicted the postbuckling response of the alumina/aluminium FGM plate, subjected to thermal and mechanical loadings, using fast converging finite double Chebyshev polynomials. Lee *et al*[26] investigated the postbuckling behavior of FGM ceramic-metal plates under edge compression and temperature field conditions using element free kp-Ritz method.

Besides simulating the FGMs with continuously varying material properties, researchers have also adopted the layer-wise approximation of graded material properties of FGMs for structural analysis of FGM plate and FGM shell[27–34]. For instance, the layer-wise finite element formulation for static and dynamic analysis of a FGM plate with surface-bonded piezoelectric layers was used by Shakeri and Mirzaeifar[27]. Cinefra and Soave[28] used the layer-wise formulation to obtain closed form solutions of free vibration of simply-supported FGM plates. Shao[29] obtained the solutions of temperature, displacements, and thermal/mechanical stresses in a functionally graded circular hollow cylinder by using a multi-layered approach based on the theory of laminated composites. Very recently, Yaghoobi *et al*[30] investigated the thermal buckling response of functionally graded materials (FGMs) with surface-bonded piezoelectric actuators under uniform temperature rise and constant actuator voltage using layer wise model of FGMs. A multilayered model of FGMs is also utilized by Jin[31] in order to obtain the transient heat conduction behavior of FGM strip.

Relatively little efforts have been made in the past by the researchers and the investigators to study the buckling and postbuckling behavior of FGM plate with geometric irregularities. For instance, Zhao *et al*[35] presented results on thermal and mechanical buckling analysis of FGM plate with circular and square cutouts using the element-free kp-Ritz method. Lal *et al*[36] developed a FEM model for stochastic mechanical and thermal postbuckling response of FGM panels with circular and square holes having material randomness. Natarajan *et al*[37] investigated the buckling behavior of FGM plate containing geometrical flaws in the form of crack and cutouts. Abolghasemi *et al*[38] conducted FEM study on the effect of the elliptical cutout on thermo-mechanical buckling response of FGM plate by drawing stability

diagrams. Among very recent attempts, Shaterzadeh *et al*[39] investigated the buckling behavior of FGM plate with multiple cutouts of various shapes under uniform temperature rise, whereas Yu *et al*[40] utilized a numerical method based on extended isogeometric analysis to study the thermal buckling behavior of FGM plate with internal defects (e.g., crack or cutout).

Although most of the FGMs applications involve high temperature environments combined with various mechanical loads, but practical scenario may involve pure mechanical loading as well. As evident from the above literature study, in contrast with thermal and thermo-mechanical loadings, very little work has been done to predict the response of FGM plates with a central hole subjected to pure mechanical loadings, especially using finite element approach. Further, most of the investigations on postbuckling behavior of FGM plates are concerned with the study of the load versus out-of-plane deflection relationship under various loading and boundary conditions; however, no concern has been shown in predicting the failure load of FGM plates. Hence in the present paper a layer-wise nonlinear FEM formulation for FGM plate, based on the first-order shear deformation theory and the von-Karman's nonlinear kinematics, is presented to examine the effects of various parameters, viz, material in-homogeneity (power exponent *n*), slenderness ratio (*b*/*h*), boundary conditions (SSSS, SCSC and CCCC), hole size (*d*/*b* ratio) and loading conditions (uniaxial and biaxial in-plane compression), on the bucking and postbuckling behavior, and the failure response of FGM plate with a central circular hole under in-plane compressive load.

2 Approach and Problem Definition

2.1 Modeling approach for FGM plate

Figure 1 shows a FGM plate, consisting of two constituent materials (ceramic and metal), measuring *a*, *b* and *h* as length, width and thickness, respectively. A coordinate system (*x*, *y*, *z*) is established on the middle plane of the plate. The volume fraction of the material constituents is assumed to follow a simple power law distribution in the thickness direction only.

In the present study, the actual non-homogeneous (in thickness direction) FGM plate with continuously varying properties along thickness is modeled as a laminate composed of multiple perfectly-bonded layers of isotropic material having layer-wise constant composition, as used in earlier studies[27–33].

2.2 Effective material properties and failure criterion for FGM

FGMs are inhomogeneous materials of smoothly varying ceramic/metallic mixture ratio through the thickness. The volume fractions of ceramic and metallic constituents are assumed to follow, the power law distribution as:

$$V_m(z) = \left(\frac{z}{h} + \frac{1}{2}\right)^n ; V_c(z) = 1 - V_m(z) \quad \ldots (1)$$

where *V* denotes the volume fraction of constituents. The subscripts *c* and *m,* respectively, correspond to the ceramic and the metallic constituents. *n* is a variable called power law exponent, which determines the material variation profile through the plate thickness-coordinate, *z* varying from $-h/2\ to\ h/2$.

The continuously varying mechanical properties, such as elastic constants, and yield stress of FGM can be depicted by a homogenized mixture rule, so called TTO model (also called the modified rule of mixtures). The TTO model, initially proposed and used for metal alloys (Fe-Ni-C) by Tamura *et al* [41], has been modified for FGMs by introducing a proper stress transfer parameter[42,43] and applied by many researchers in the study of FGM. For instance, Jin *et al*[44] investigated the nucleation of plastic crack growth near the interface of metal/ceramic FGM using TTO model. Williamson *et al*.[45] adopted TTO model to investigate residual stresses developed at the interfaces of Al_2O_3-Ni. Giannakopoulos *et al*[46] investigated the elastoplastic response of Al_2O_3-Ni FGM layer using the incremental theory of plasticity and the stress-strain curves for FGM were drawn by using TTO model. Very recently, few attempts[47–49] have also been made to investigate the elastoplastic buckling and/or postbuckling behavior of FGM plates and shells using TTO model.

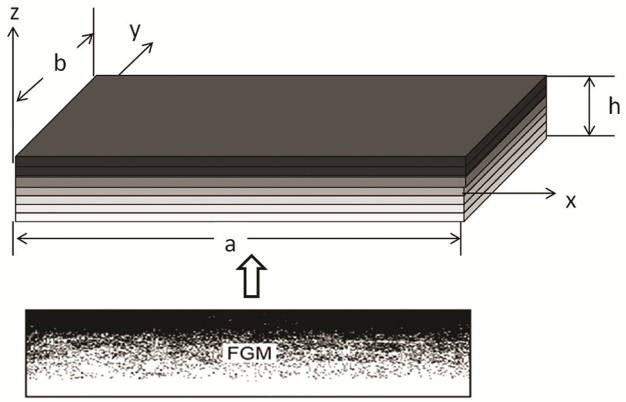

Fig. 1 — Modeling of actual non-homogeneous FGM plate into a laminate composed of multiple perfectly-bonded homogeneous layers

In TTO model the effective Young's modulus of two-phase materials, like FGM is given in terms of Young's modulii (E_c and E_m) and volume fractions (V_c and V_m) of respective phases (ceramic and metallic phases), as follows

$$E(z) = \left\{V_m(z)E_m\frac{q+E_c}{q+E_m} + (1-V_m(z))E_c\right\} \times \left\{V_m(z)\frac{q+E_c}{q+E_m} + (1-V_m(z))\right\}^{-1} \quad \ldots (2)$$

where the subscripts *c* and *m* correspond to the material phases ceramic and metal, respectively; and, *q* represents the stress transfer parameter, also called stress-to-strain transfer ratio. The value of *q*, determined numerically or/and experimentally, depends upon the properties of constituent materials as well as on the microstructure interaction in FGM material. For Ni-Al_2O_3[46] and TiB/Ti[44] FGMs, the values for *q* are found to be 4.5 GPa, and for FGM containing Al and SiC[50,51] phases it is determined to be 91.6 GPa. The Poisson's ratio is assumed to be constant along the thickness of the FGM plate.

It is to be noticed that the TTO model assumes that the overall failure behavior of two-phase composite containing both brittle and ductile phases is governed by the ductile constituent[44]. This assumption is also considered to be reasonable in the case of FGMs (containing ceramic: a brittle phase, and metal: a ductile phase) because the ductility and good shear strength induced in the FGM by the metal phase relax the stress concentration induced around the inherited cracks and flaws of ceramics through the plastic deformation and hence, eliminate the possibility of brittle failure of FGM[52,53]. Therefore, based on the assumption that the FGM composite yields once the metal constituent yields, the TTO model uses *q* to give overall yield strength of FGM composite in terms of yield strength of ductile metallic phase (σ_{ym}) as:

$$\sigma_y(z) = \sigma_{ym}\left[V_m(z) + \left(\frac{q+E_m}{q+E_c}\right)\frac{E_c}{E_m}(1-V_m(z))\right] \ldots (3)$$

Using the volume fraction of constituents at a particular value of thickness coordinate (calculated from Eq. (1)), the Young modulus and the yield strength of FGM plate at that thickness coordinate are calculated using Eqs. (2) and (3). Under the assumption that FGM fails just before the elastoplastic stage, an attempt is also made to predict the failure load of FGM plate based on 3-D von-Mises criterion.

2.3 Mathematical formulation

2.3.1 Kinematic relations

In the Mindlin plate theory, the displacement $u = [u, v, w]^T$ at (*x*, *y*, *z*) are expressed as functions of the mid-plane (*z* = *0*) translations u_0, v_0, w_0 and independent normal rotations θ_x and θ_y in the *xz*- and *yz*-planes, respectively:

$$u(x,y,z) = u_0(x,y) + z\theta_x(x,y)$$
$$v(x,y,z) = v_0(x,y) + z\theta_y(x,y)$$
$$w(x,y,z) = w_0(x,y) \quad \ldots (4)$$

Incorporating the von-Karman's assumptions to write the Green's strain components for moderately large deformations into following form[54]:

$$\varepsilon_x = \frac{\partial u_0}{\partial x} + z\left(\frac{\partial \theta_x}{\partial x}\right) + \frac{1}{2}\left(\frac{\partial w_0}{\partial x}\right)^2$$
$$\varepsilon_y = \frac{\partial v_0}{\partial y} + z\left(\frac{\partial \theta_y}{\partial y}\right) + \frac{1}{2}\left(\frac{\partial w_0}{\partial y}\right)^2$$
$$\gamma_{xy} = \frac{\partial u_0}{\partial y} + \frac{\partial v_0}{\partial x} + z\left(\frac{\partial \theta_x}{\partial y} + \frac{\partial \theta_y}{\partial x}\right) + \left(\frac{\partial w_0}{\partial x}\frac{\partial w_0}{\partial y}\right)$$
$$\gamma_{xz} = \frac{\partial w_0}{\partial x} + \theta_x$$
$$\gamma_{yz} = \frac{\partial w_0}{\partial y} + \theta_y \quad \ldots (5)$$

Rewriting the Eq. (1) into matrix form:

$$\{\epsilon\} = \{\epsilon^0\} + z\{K\} \quad \ldots (6)$$

where

$$\{\epsilon\} = [\epsilon_x, \quad \epsilon_y, \quad \gamma_{xy}, \quad \gamma_{xz}, \quad \gamma_{yz}]^T \quad \ldots (7)$$

$$\{\epsilon^0\} = \left[\epsilon_x^0, \quad \epsilon_y^0, \quad \gamma_{xy}^0, \quad \gamma_{xz}^0, \quad \gamma_{yz}^0\right]^T \quad \ldots (8)$$

$$\{\epsilon^0\} = \left\{\epsilon_l^0\right\} + \left\{\epsilon_{nl}^0\right\} \quad \ldots (9)$$

in which,

$$\left\{\epsilon_l^0\right\} = \left[\frac{\partial u_0}{\partial x}, \quad \frac{\partial v_0}{\partial y}, \quad \frac{\partial u_0}{\partial y} + \frac{\partial v_0}{\partial x}, \quad \frac{\partial w_0}{\partial x} + \theta_x, \quad \frac{\partial w_0}{\partial y} + \theta_y\right]^T \left\{\epsilon_{nl}^0\right\} = \left[\frac{1}{2}\left(\frac{\partial w_0}{\partial x}\right)^2, \quad \frac{1}{2}\left(\frac{\partial w_0}{\partial y}\right)^2, \quad \left(\frac{\partial w_0}{\partial x}\frac{\partial w_0}{\partial y}\right)\right] \quad \ldots (10)$$

and,

$$\{K\} = \left[K_x, \quad K_y, \quad K_{xy}, \quad 0, \quad 0\right]^T = \left[\frac{\partial \theta_x}{\partial x}, \quad \frac{\partial \theta_y}{\partial y}, \quad \frac{\partial \theta_x}{\partial y} + \frac{\partial \theta_y}{\partial x}, \quad 0, \quad 0\right]^T \quad \ldots (11)$$

where the suffix '*l*' and '*nl*' stand for the linear and nonlinear parts, respectively, of the mid plane strain components.

2.3.2 Constitutive relations

Based on the assumptions that σ_z is negligible, the stress-strain relations are given by:

$$\begin{bmatrix}\sigma_x\\ \sigma_y\\ \tau_{xy}\\ \tau_{yz}\\ \tau_{xz}\end{bmatrix}=\begin{bmatrix} Q_{11} & Q_{12} & 0 & 0 & 0\\ & Q_{22} & 0 & 0 & 0\\ & & Q_{33} & 0 & 0\\ Symmetric & & & k_1^2Q_{44} & 0\\ & & & & k_2^2Q_{55}\end{bmatrix}\begin{Bmatrix}\epsilon_x\\ \epsilon_y\\ \gamma_{xy}\\ \gamma_{xz}\\ \gamma_{yz}\end{Bmatrix}, \quad \ldots (12)$$

where, k_1 and k_2 are shear correction factors and Q_{ij} are the reduced stiffness for plane stress case and are function of material properties as follows:

$$Q_{11}=\frac{E(z)}{1-\nu^2}, Q_{12}=\nu Q_{11}, Q_{22}=Q_{11},$$
$$Q_{44}=Q_{55}=\frac{E(z)}{(1+\nu)}, \quad \ldots (13)$$

where $E(z)$ is the Young's modulus that varies across the thickness of FGM plate according to Eq. (2), and ν is the Poisson's ratio that is assumed to be constant through the thickness of FGM plate.

2.3.3 FEM approach

FGM plate is meshed with nine-noded Lagrangian elements having five degrees of freedom per node, as used by many researchers for the study of laminated composite plates[9-10]. From the principle of virtual work and the total Lagrangian approach, the element level nonlinear equilibrium equation is derived as[54]:

$$\psi\{a\}=\int_A\left[[B_0]^T\{N\}+[B_b]^T\{M\}+[B_s]^T\{Q\}\right]dA-R=0, \quad \ldots (14)$$

where, $\psi\{a\}$ is the residual force which is a function of nodal displacement vector $\{a\}$; B_0, B_b, and B_b are the strain-displacement matrices corresponding to in-plane axial, bending and shear strains, respectively; $\{N\}$ is the stress resultants per unit length; $\{M\}$ is the moment resultants per unit length; $\{Q\}$ represents the transverse shear stress resultants per unit length; and, R is the in-plane external applied loads.

As a result of FEM formulation, the developed nonlinear algebraic equations are solved using Newton-Raphson method, wherein the numerical stability and convergence of the solution are obtained by applying the load in small increments. A selective integration scheme (i.e., 3×3 integration rule to integrate the functions related to the membrane and the bending behavior, and 2×2 integration rule for the transverse shear terms) is used to avoid the shear locking problem. The value of five stress components (three in-plane stresses and two transverse shear stresses) to be supplied in 3-D von-Mises criterion, are calculated at mid thickness of each layer of individual element using the constitutive equations[5-6].

2.4 Problem definition

2.4.1 Material properties and geometric model

In the present study, nonlinear finite element analysis of a rectangular FGM plate of dimension ($a \times b \times h$) with centrally located circular hole of different *d/b* ratios (where *d* refers to the diameter of circular hole and b the width of FGM plate) is carried out to study its buckling and postbuckling responses, and failure load. The FGM plate is assumed to be made of two constituents: TiB (ceramic phase) and Ti (metallic phase). Following material properties are taken for the ceramic and metallic phases of FGM[39]: E_C = 375GPa, E_m = 107 GPa, $\nu = 0.24$ (for ceramic and metal both) and σ_{ym} = 400 MPa. The value of q, the stress transfer parameter[39], is taken as 4.5 GPa.

2.4.2 Boundary and loading conditions

The current study is carried out for the FGM plate with flexural boundary conditions (BCs) to be clamped on all edges (CCCC), except for the case where effects of BCs are studied; wherein, in addition to CCCC (clamped at all edges), following three sets of flexural BCs are considered:

SCSC: simply-supported at $y = 0$ & b edges and clamped at other two edges (i.e., at $x = 0$ and $x = a$); SSSS: simply-supported at all edges.

It is to be noted that in all the above cases of BCs, the in-plane boundary conditions on edges $x = 0$, $x = a$, $y = 0$ and $y = b$ (as depicted in Fig. 2) related to in-plane displacements in *x*- and *y*-directions (u and v, respectively) are taken to be same.

Two types of in-plane and uniformly distributed loading conditions are considered: uniaxial (only in *x*-direction) compression load applied on edge $x = a$, with constraining the in-plane movement in *x*-direction at edge $x = 0$, whereas the in-plane movements in *x*- and *y*-directions at edges $x = 0$ and $y = 0$ are constrained while applying the biaxial (in *x*- and *y*-directions) compression loads on edges $x = a$ and $y = b$. Results for buckling and failure loads and the transverse deflection are presented in the following non-dimensional forms:

In-plane buckling and failure load: $\frac{N_{x\,(or\,y)}\,b^2}{E_c h^3}$

Maximum transverse deflection: $\frac{w_{max}}{h}$

where E_c represents the Young's modulus of ceramic; h the thickness of FGM plate; b the width of plate; $N_{x\,(or\,y)}$ the in-plane compressive load in x-direction (or y-direction)

3 Convergence Study

To fix the number of elements in the finite element mesh and the number of layers to model the FGM plate, a convergence study was conducted for a clamped (CCCC), square Ti/TiB FGM (for n = 1) plate with centrally located circular hole of size d/b = 0.1

The convergence of buckling and failure loads was checked under uniaxial compressive load and the results are given in Table 1. It can be observed from Table 1 that a reasonably good convergence of buckling loads and failure loads is obtained for the mesh of 120 elements having 30 layers. Schematic of finite element mesh along with element-and node-numbering schemes for a typical FGM plate with circular hole is shown in Fig. 2.

Table 1 – Results of convergence study for critical buckling load $\left(\boldsymbol{\lambda = \frac{N_x b^2}{E_c h^3}}\right)$ and failure load $\left(\boldsymbol{\lambda^* = \frac{N_{fail} b^2}{E_c h^3}}\right)$

Number of elements	Number of layers							
	10		20		30		40	
	λ	λ^*	λ	λ^*	λ	λ^*	λ	λ^*
48	4.5495	5.6965	4.5113	5.6583	4.5113	5.6200	4.5016	5.5698
72	4.4540	5.8876	4.2054	5.5818	4.0525	5.5053	4.1201	5.3409
96	4.2054	5.7347	4.1672	5.4671	4.1672	5.4671	4.1290	5.3409
120	4.1672	5.6583	4.1290	5.3906	4.1290	5.2759	4.1290	5.2646
144	4.1672	5.5818	4.1290	5.3142	4.1290	5.2377	4.1290	5.2646

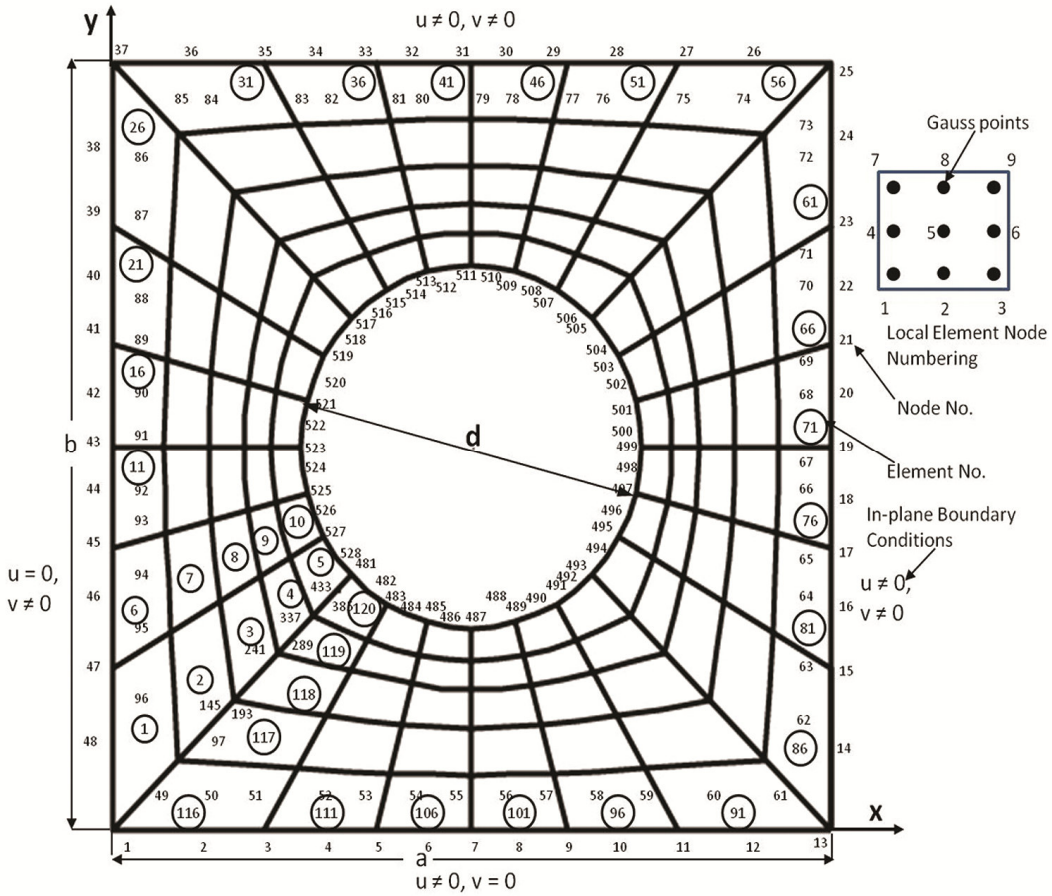

Fig. 2 — Meshing of a typical FGM plate with a circular hole along with in-plane boundary conditions

4 Verification of Results

The accuracy of the developed program is checked by comparing the results obtained using the present formulation with the results available in the existing literature. A thin square plate (*b/h=100*) containing a central circular hole (of various sizes) under in-plane (uniaxial and biaxial) compressive loading conditions is considered to make the comparison of results with those published by Sabir and Chow[7]. The plate is considered to be made of an isotropic and homogenous material with Young's modulus, E = 207 GPa and Poisson's ratio, ν = 0.3, (same as used in Ref.[7]). Buckling load (normalized as: $\frac{12(1-\nu^2)}{\pi^2}\frac{N_{cr}b^2}{Eh^3}$) are compared for simply-supported and clamped edge boundary conditions. The results of comparison are shown in Table 2. It can be observed that the results obtained from the present work are in good agreement with the results as reported by Sabir and Chow [7].

5 Numerical Studies

Various numerical studies are conducted in this paper to examine the effects of different parameters, viz. material in-homogeneity (power exponent n), slenderness ratio (b/h), boundary conditions (SSSS, SCSC and CCCC), hole size (d/b ratio) and loading conditions (uniaxial and biaxial in-plane compression) on the bucking and postbuckling behavior, and the failure response of FGM plate. A Ti/TiB FGM square plate (of side 279 mm) with a central circular hole is considered. It is to mention here that material is graded as per TTO model as specified in Section 2.3, i.e., using the volume fraction of the constituents at a particular value of thickness coordinate (calculated using Eq. (1)), the Young's modulus and the yield strength of FGM plate at that thickness coordinate are calculated using Eqs. (2) and (3), respectively.

Table 2 — Verification of results

Boundary condition	Loading condition	d/b ratio	Normalized buckling load $\left(\frac{12(1-\nu^2)}{\pi^2}\frac{N_{cr}b^2}{Eh^3}\right)$	
			Present study	Ref[7]
SSSS	uniaxial	0.1	3.81	3.80
		0.3	3.19	3.20
		0.5	2.91	2.90
	biaxial	0.1	1.91	1.88
		0.3	1.77	1.75
		0.5	1.66	1.65
CCCC	uniaxial	0.1	9.40	9.45
		0.3	8.93	9.04
		0.5	10.90	9.40
	biaxial	0.1	5.07	4.88
		0.3	5.27	5.10
		0.5	7.86	7.60

Table 3 — Critical buckling load $\left(\lambda = \frac{N_x b^2}{E_c h^3}\right)$, failure load $\left(\lambda^* = \frac{N_{fail} b^2}{E_c h^3}\right)$ and maximum transverse deflection $\left(\frac{w_{max}}{h}\right)$ of the square CCCC Ti/TiB FGM plate with circular hole of size d/b=0.1 under uniaxial compression

n	λ	λ^*	$\frac{w_{max}}{h}$
0	2.39	4.11	1.89
1	4.13	5.27	1.14
2	4.74	6.11	1.15
3	5.16	6.61	1.12
10	6.46	7.99	1.04

6 Results and Discussion

6.1 Effect of material in-homogeneity

FGM with different material in-homogeneity is obtained by varying volume fraction through the thickness using Eq. (1) for different values of exponent n (0, 1, 2, 3, and 10). A CCCC FGM plate with a circular hole is studied under uniaxial compression. The width-to- thickness ratio (slenderness ratio, b/h) was taken to be 200. The ratio of diameter of circular hole to width of the plate (d/b) is taken as 0.1. The corresponding results are given in Table 3 and plotted in Fig. 3. Figure 3 and Table 3 depict higher value of critical buckling and failure loads corresponding to FGM plate (for $n > 0$) as compared to that of pure metal plate (for $n = 0$). At this point, it is necessary to mention that the proportions of constituent materials through the thickness of FGM plate are controlled by

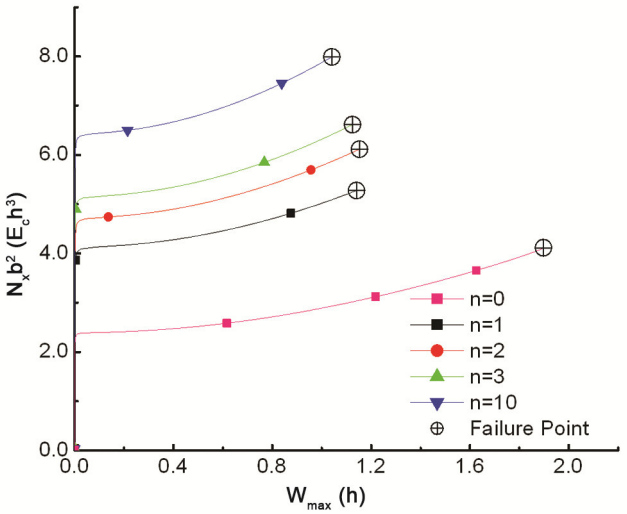

Fig.3 — Effect of power law exponent (n) on postbuckling response of square Ti/TiB FGM plate with a circular hole (of d/b = 0.1) under uniaxial compression.

the value of power law exponent n in Eq. (1). Higher value of n means high proportion of TiB which possess higher buckling and failure strengths as compared to that of metal constituent and hence, the buckling and failure strength of the resulting FGM plate are increased. It is further to note from Fig. 3 that the FGM plate also possesses reserved postbuckling strength, whereas the FGM has same postbuckling stiffness (given by the slope of the load-deflection curve at a particular value of deflection) as that of metal constituent. Moreover, it is also to report that for FGM ($n > 0$) the failure takes place at the hole edges, whereas it occurs at the outer edges of the plate for n = 0 (in the case of pure metal).

6.2 Effect of slenderness ratio

Results of effect of slenderness ratio (b/h) on buckling and postbuckling behavior and the failure of clamped FGM (for n = 1) plate with a circular hole (of *d/b=0.1*) under uniaxial compression are shown in Table 4 and Fig. 4. The various values of slenderness ratio taken are 50, 100, 150, 200 and 300. It is necessary to mention here that while carrying out the study on the effects of slenderness ratios; the number of layers was increased proportionally based on the convergence study conducted in Section 3.0 to get the converged results. For example, for b/h = 100, the numbers of layers were taken as 60, as against 30 for b/h = 200 calculated in the convergence study carried out in Section 3. As observed from Fig. 4 and Table 4 that although the effect of b/h is not evident in the non-dimensional load-deflection plots (because of the presence of b/h term in non-dimensional form), but the effect of b/h ratio is very significant on dimensional values of critical buckling and failure loads, as observed in Table 4.

It can also be observed from Fig. 4 and Table 4 that the in FGM plate with slenderness ratios equal to 50 and 100, failure occurs before the buckling starts; for all other cases (b/h = 150, 200 and 300) the FGM fails in postbuckling region after critical buckling.

The current findings explain that thin FGM plate is expected to buckle before the stresses reach to a critical level as defined by the criterion, whereas thick FGM plate would fail before buckling because of large stresses developed inside the FGM. Furthermore, Table 4 shows that the dimensional values of buckling (for $b/h > 100$) and failure loads are decreased considerably with the decrease in the thickness of FGM plate (with the increase in b/h). It is to mention here that the observed location of failure in FGM plate for all slenderness ratios remains same at hole edge, except for b/h = 300 wherein the failure occurs at the outer edge of FGM plate.

Table 4 — Effect of slenderness ratio (b/h) on critical buckling load and failure load of the square CCCC TiB/Ti FGM plate (n = 1) under uniaxial compression with a circular hole.

b/h	Buckling load		Failure load	
	Dimensional (kN)	Non-dimensional	Dimensional (kN)	Non-dimensional
50*	854.57	1.02	449.97	0.53
100*	359.99	3.44	219.99	2.10
150	127.49	4.11	128.49	4.14
200	54.00	4.13	68.99	5.27
300	16.50	4.25	33.99	8.77

*In the cases of b/h =50 and 100 failure would take place before buckling.

6.3 Effect of hole size

The effect of circular hole size (d/b = 0.1, 0.2, 0.3, 0.4 and 0.5) on the responses of clamped FGM (for n = 1) plate (with b/h = 200) under uniaxial compression load are also investigated and the corresponding results are shown in Table 5 and Fig. 5.

It can be observed from Fig. 5 and Table 5 that the buckling load decreases slightly with an increase in d/b ratio up to 0.3, but subsequently the buckling load start increasing with the increase in d/b ratio. As against the conventional wisdom, this peculiar phenomenon of increase in buckling load of FGM plate with large hole as compared to small hole size can be explained as follows. When the hole size becomes greater than d/b = 0.3, it affects the load carrying pattern of the plate with most of the

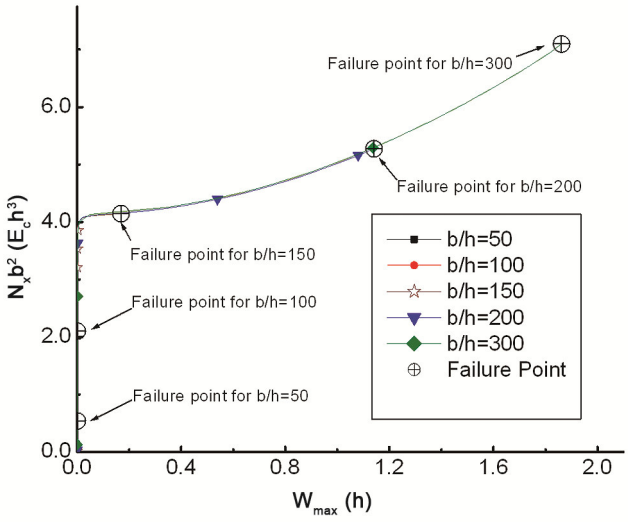

Fig. 4 — Effect of slenderness ratio on postbuckling and failure behavior of FGM plate under uniaxial compression.

compressive load carried by the narrow side strips of material along the clamped boundaries of the plate.

It is worth mentioning that similar anomalous findings of increase in buckling load with increase in the hole size have been reported by many other investigators/researchers for the cases of both composite and isotropic plates for a right combination of boundary conditions and plate's aspect ratio[5,55–59]. For instance, Ritchie and Rhoades[58] found that presence of perforation in isotropic plate does not reduce the buckling load always, and in some instances may increase the buckling load of plate. In addition, this peculiar notion has been verified both numerically and experimentally for orthotropic laminated plates by Nemeth[55]. Very lately, Prajapat *et al*[59] examined the buckling behavior of isotropic perforated plate and concluded that the unrestrained edges of cutout make the plate free to move laterally and causes tensile stresses or comparatively low compressive stresses in the middle region of the plate which results in a buckling load that is even higher than the buckling load of the plate with no cutout. Further, this peculiar notion has been verified for perforated FGM plate by Abolghasemi *et al*[38]. A monotonic decrement in the failure load, associated transverse deflection and postbuckling stiffness with an increase in hole size, can also be noticed from Fig. 5 and Table 5.

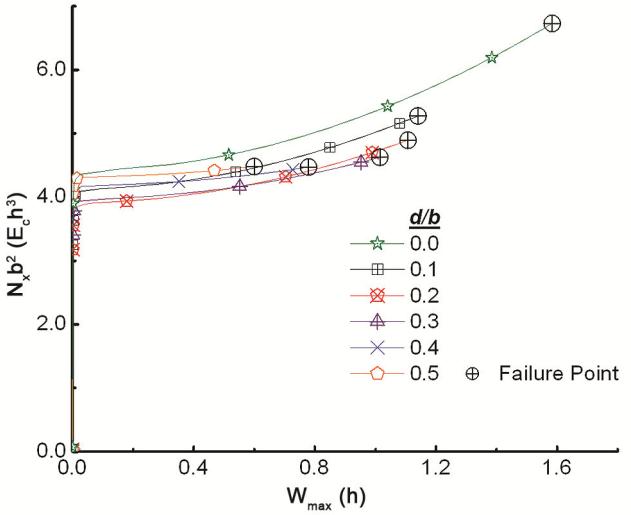

Fig. 5 — Effect of hole size on buckling and postbuckling responses and failure load of square Ti/TiB FGM (n=1) plate with a circular hole under uniaxial compression.

Table 5 — Effect of hole size on buckling and failure characteristics of square Ti/TiB FGM (n = 1) plate with a circular hole under uniaxial compression.

d/b	λ	λ^*	$\frac{w_{max}}{h}$
0.0	4.43	6.72	1.58
0.1	4.12	5.27	1.14
0.2	3.93	4.89	1.10
0.3	3.97	4.62	1.01
0.4	4.20	4.47	0.77
0.5	4.32	4.48	0.60

6.4 Effect of boundary conditions

Figure 6 contains the plots corresponding to the effects of boundary conditions (SSSS, SCSC and CCCC) on the bucking and postbuckling behavior, and the failure response of FGM (for n = 1) plate (b/h = 200) with a circular hole of size d/b = 0.1 under uniaxial compression. It can be observed from Fig. 6 that CCCC plate depicts highest buckling and postbuckling strength (for a particular value of deflection) and failure load whereas for SSSS plate the values are the lowest. The maximum transverse deflection at the time of failure is minimum for CCCC plate condition, and it is maximum for SSSS boundary condition. These findings can also be attributed to the fact that increase in the rigidity of supports on the edges of FGM plate results in the increase of buckling and postbuckling strengths and failure load, and the decrease in transverse deflection.

6.5 Effect of loading conditions

The effects of loading conditions (in-plane uniaxial and biaxial compression) on the buckling and postbuckling responses, and failure of clamped FGM (for n = 1) plate (of b/h = 200) with a circular hole of size d/b = 0.1 are investigated, and the corresponding

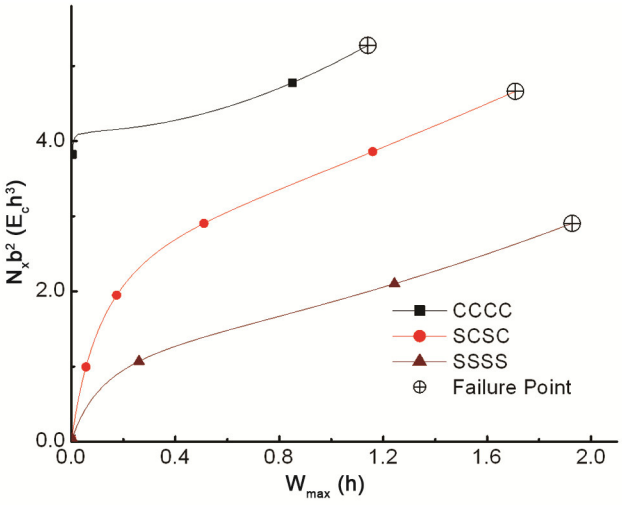

Fig. 6 — Load-deflection response and failure of FGM plate with different boundary conditions.

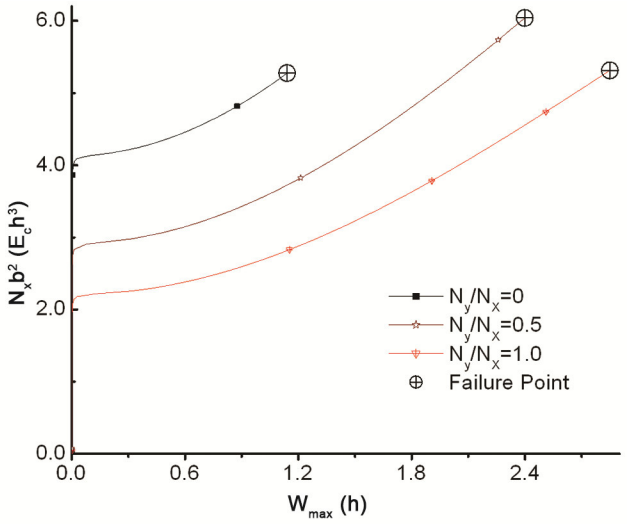

Fig. 7 — Load-deflection response of CCCC Ti/TiB FGM (for n = 1) plate under in-plane uniaxial and biaxial compression.

results are plotted in Fig. 7. The results show that maximum buckling load is obtained for plate under uniaxial compression (for $N_y/N_x = 0$) and the postbuckling load-deflection curves become significantly lower as the value of N_y is increased.

7 Conclusions

Based on the present formulation and the various numerical studies conducted on Ti/TiB FGM square plate with a central circular hole to examine the effects of various parameters, viz, material in-homogeneity (power exponent n), slenderness ratio (b/h), boundary conditions (SSSS, SCSC and CCCC), hole size (d/b ratio) and loading conditions (uni-axial and bi-axial in-plane compression) on the bucking and postbuckling behavior, and the failure response of FGM plate, the following important conclusions can be drawn:

(i) Buckling load and reserved postbuckling strength of perforated FGM plate increase monotonically with an increase in power law exponent n, whereas the postbuckling stiffness of FGM plate at all values of transverse deflection is same as that of metal plate (n = 0).

(ii) Thin FGM plate is found to be vulnerable towards buckling failure, whereas the thick FGM plate fails because of large stresses developed before buckling.

(iii) In the case of FGM plate with larger hole size, the rigid clamped conditions at the boundary edges of the FGM plate are found to provide the required rigidity to increase its buckling load as compared to smaller hole size.

(iv) Increase in the hole size results in a monotonic decrement in the failure load, maximum transverse deflection and postbuckling stiffness of FGM plate.

References

1 Suresh S & Mortensen A, *Fundamentals of functionally graded materials*, (The Institut of Materials), 1998.
2 Shiota I & Miyamoto Y, *Functionally graded materials,* (Elsevier), 1996.
3 Reddy J N, *Int J Numer Methods Eng*, 47 (2000) 663.
4 Reddy J N & Chin C D, *J Therm Stress*, 21 (1998) 593.
5 Arbocz J, Potier M, Singer J & Tvergaard V, *Buckling and Post-buckling: Four lectures in experimental, numerical and theoretical solid mechanics based on talks given at the CISM-meeting Held in Udine,* Italy, 1985, (Springer-Verlag), 1987.
6 Singh S B & Kumar A, *Compos Sci Technol*, 59 (1999) 727.
7 Sabir A B & Chow F Y, *Thin-Walled Struct*, 4 (1986) 135.
8 Marshall I, Little W & Tayeby M, in M*echanical characterization of load bearing fiber composite laminates*, (Elsevier Applied Science Publishers), 1985.
9 Kumar D & Singh S B, *Compos Struct*, 92 (2010) 769.
10 Kumar D & Singh S B, *Compos Part B Eng*, 43 (2012) 142.
11 Birman V, *Compos Eng*, 5 (1995) 913.
12 Feldman E & Aboudi J, *Compos Struct*, 38 (1997) 29.
13 Lanhe W, *Compos Struct*, 64 (2004) 211.
14 Javaheri R & Eslami M, *AIAA J*, 40 (2002) 162.
15 Najafizadeh M & Eslami M, *AIAA J,* 40 (2002) 1444.
16 Samsam B & Eslami M R, *Int J Solids Struct*, 43 (2006) 4082.
17 Matsunaga H,*Compos Struct*, 90(2009) 76.
18 Liew K M, Yang J & Kitipornchai S, *Int J Solids Struct*, 40 (2003) 3869.
19 Yang J & Shen H, *Int J Non Linear Mech*, 38 (2003) 467.
20 Woo J, Meguid S, Stranart J C & Liew K M, *Int J Mech Sci,* 47 (2005) 1147.
21 Na K S & Kim J H, *Compos Part B Eng*, 35 (2004) 429.
22 Na K S & Kim J H, *Finite Elem Anal Des*, 42 (2006) 749.
23 Shen H S, *Int J Mech Sci,* 49 (2007) 466.
24 Duc D & Tung V, *Mech Compos Mater*, 46 (2010) 461.
25 Wu T L, Shukla K K & Huang J H, *Compos Struct*, 81 (2007) 1.
26 Lee Y Y, Zhao X & Reddy J N, *Comput Methods Appl Mech Eng*, 199 (2010) 1645.
27 Shakeri M & Mirzaeifar R, *Mech Adv Mater Struct*, 16 (2009) 561.
28 Cinefra M & Soave M, *Mech Adv Mater Struct*, 18 (2011) 3.
29 Shao Z S, *Int J Press Vessel Pip*, 82 (2005) 155.
30 Yaghoobi H, Fereidoon A, Khaksari M & Mareishi S, *Mech Adv Mater Struct*, 22 (2015) 864.
31 Jin Z H, *Int Commun Heat Mass Transf,* 29 (2002) 887.
32 Shakeri M, Akhlaghi M & Hoseini S M, *Compos Struct*, 76 (2006) 174.

33 Cinefra M, Carrera E, Brischetto S & Belouettar S, *J Therm Stress*, 33 (2010) 942.

34 Kapuria S, Bhattacharyya M & Kumar A N, *Compos Struct*, 82 (2008) 390.

35 Zhao X, Lee Y Y & Liew K M, *Compos Struct*, 90 (2009) 161.

36 Lal A, Singh H & Shegokar N L, *Int J Mech Sci*, 62 (2012) 18.

37 Natarajan S, Chakraborty S, Ganapathi M & Subramanian M, *Eur J Mech A/Solids,* 44 (2014) 136.

38 Abolghasemi S, Shaterzadeh A R & Rezaei R, *Aerospace Sci Technol*, 39 (2014) 250.

39 Shaterzadeh A R, Rezaei R & Abolghasemi S, *J Therm Stress*, 38 (2015) 1250.

40 Yu T, Bui T Q, Yin S, Doan D H, Wu C T, Van T & Tanaka S, *Compos Struct*, 136 (2015) 684.

41 Tamura I, Tomato Y & Ozawa H, *Proc Third Conf Strength Met Alloy*, 1 (1973) 611.

42 Tohgo K, Masunari A & Yoshida M, *Compos Part A Appl Sci Manuf*, 37 (2006) 1688.

43 Bocciarelli M, Bolzon G & Maier G, *Comput Mater Sci*, 43 (2008) 16.

44 Jin Z H, Paulino G H & Dodds R H, *Eng Fract Mech*, 70 (2003) 1885.

45 Williamson R L, Rabin B H & Byerly G E, *Compos Eng*, 5 (1995) 851.

46 Giannakopoulos A E, Suresh S, Finot M & Olsson M, *Acta Metall Mater*, 43 (1995) 1335.

47 Fu Y, Shao X & Chen Y, *Appl Math Mech*, 35 (2014) 325.

48 Huang H, Chen B & Han Q, *Compos Struct*, 118 (2014) 234.

49 Zhang Y, Huang H & Han Q, *Compos Part B Eng*, 69 (2015) 120.

50 Gunes R, Aydin M, Apalak M K & Reddy J N, *Compos Struct*, 93 (2011) 860.

51 Bhattacharyya M, Kapuria S & Kumar A N, *Mech Adv Mater Struct*, 14 (2007) 295.

52 Soh A K, Bian L C & Chakrabarty J, *Thin-Walled Struct*, 38 (2000) 247.

53 Bandyopadhyay A, Atisivan R, Kuhn G & Yeruva S, *Proc. SFF Texas*, 1 (2000) 24.

54 Reddy J N, *An introduction to nonlinear finite element analysis*, (Oxford University Press), 2004.

55 Nemeth M P, *Buckling and postbuckling behaviour of laminated composite plates with a cut-out*, (Springer), 1995.

56 Soares C G, *Ships Offshore Struct*, 6 (2011) 1.

57 Hu H T & Lin B H, *Compos Sci Technol*, 55 (1995) 277.

58 Ritchie D & Rhodes J, *Aeronaut Q*, 26 (1975) 281.

59 Prajapat K, Chaudhuri S & Kumar A, *Thin Walled Struct*, 90 (2015) 171